Nonadiabatic Molecular Dynamics on Real-Time Excited-State Surfaces via Machine Learning Hamiltonians

Changwei Zhang,[1] Yang Zhong,[1] Zhi-Guo Tao,[1] Yingzhou Li,[2] Zhenggang Lan,[3] Oleg V. Prezhdo,[4] Xin-Gao Gong,[1] Weibin Chu,[1,*] and Hongjun Xiang[1,†]

[1]*Key Laboratory of Computational Physical Sciences (Ministry of Education), Institute of Computational Physical Sciences, State Key Laboratory of Surface Physics, and Department of Physics, Fudan University, Shanghai, 200433, China*

[2]*School of Mathematical Sciences, Fudan University, Shanghai, 200433, China*

[3]*SCNU Environmental Research Institute, Guangdong Provincial Key Laboratory of Chemical Pollution and Environmental Safety and MOE Key Laboratory of Environmental Theoretical Chemistry, South China Normal University, Guangzhou, Guangdong, 510006, China*

[4]*Department of Chemistry and Chemical Biology, University of New Mexico, Albuquerque, New Mexico, 87106, USA*

(Received 25 January 2026; accepted 9 July 2026; published 14 August 2026)

Simulating the coupled, nonequilibrium dynamics of electrons and nuclei is a central challenge in chemistry, physics, and materials science, governing phenomena from photocatalysis to quantum information. The primary bottleneck has been the lack of a general, accurate, and efficient method for modeling the complete excited-state landscape: the potential energy surfaces, forces, and nonadiabatic couplings for multiple electronic states. While machine learning has revolutionized ground-state simulations and shown promise for excited states in molecules, a unified framework that solves the complete multistate problem for general condensed matter systems has remained elusive. Here, we introduce on-the-fly neural network nonadiabatic molecular dynamics (NAMD), a machine learning framework that makes on-the-fly NAMD in solids a reality. By employing an equivariant neural network to predict the system Hamiltonian, the framework delivers excited-state energies, forces, and nonadiabatic coupling vectors at a fraction of the cost of *ab initio* calculations. Crucially, it allows simulations with hybrid functional accuracy, a level of approach previously inaccessible for NAMD. We showcase its capabilities with three topical examples: correcting order-of-magnitude errors in carrier dynamics predicted by conventional procedure in a MoS_2/WS_2 heterostructure, simulating previously inaccessible photo-induced ferroelectric switching, and capturing real-time polaron formation in TiO_2 at the hybrid-functional level. On-the-fly neural network NAMD moves beyond the limitations of equilibrium theory, establishing a new paradigm for the predictive, first-principles design of materials operating far from equilibrium.

DOI: 10.1103/9wbw-h87d

The coupled, nonequilibrium dynamics of electrons and nuclei constitute the microscopic foundation of modern condensed matter physics, governing phenomena ranging from photovoltaic energy conversion and photocatalysis to ultrafast optoelectronics [1–7]. However, developing predictive, first-principles theoretical frameworks capable of describing materials driven far from equilibrium remains a formidable challenge. Specifically, intense photoexcitation invalidates standard perturbative approaches, necessitating methods that treat electronic and lattice degrees of freedom on an equal footing.

Nonadiabatic molecular dynamics (NAMD), particularly via the fewest-switches surface hopping algorithm [8], has emerged as the fundamental tool for simulating such dynamics in molecules and small nanoclusters [9–11]. However, extending rigorous fewest-switches surface hopping to solids presents a significant computational challenge, as exact "on-the-fly" propagation requires calculating excited-state forces and nonadiabatic coupling vectors (NACVs) at every time step across thousands of trajectories. Consequently, solid-state NAMD has relied almost exclusively on the classical path approximation (CPA), also known as the "neglect of backreaction approximation" [12,13]. By decoupling nuclear motion from the instantaneous electronic state and treating phonons as a precomputed background, the CPA assumes that the lattice evolves exclusively on a static potential energy surface (PES), therefore replacing computationally demanding NACVs with scalar couplings along a fixed trajectory, and bypassing the need for excited-state forces. While extensively employed within the solid-state community for

*Contact author: wbchu@fudan.edu.cn
†Contact author: hxiang@fudan.edu.cn

modeling weak-field excitations, the CPA suffers from a critical physical deficiency: it entirely neglects the backreaction of excited carriers on the lattice, rendering it blind to the profound reshaping of interatomic forces under electronic excitation. As a result, the CPA collapses in the far-from-equilibrium regimes central to NAMD, failing to capture phenomena where the lattice response to the excited electron is the primary driver, such as photoinduced phase transitions, chemical reactions, ferroelectric switching, and the dynamic formation of quasiparticles (such as polarons, polaritons, and magnons). Overcoming this limitation requires restoring the essential Tully's feedback loop by explicitly evaluating excited-state forces and NACVs without incurring the prohibitive cost of *ab initio* methods. Recently, machine learning (ML) holds the potential to fundamentally reshape the landscape of NAMD simulations [14–20]. However, previous efforts in solid-state ML-NAMD [21], including our own recent work [22], have primarily focused on accelerating the CPA work flow. While separate progresses have been made in learning excited-state potentials [23,24] and nonadiabatic couplings for molecular systems [25–27], a unified framework capable of lifting the restrictions of the CPA in solids has yet to be realized.

In this Letter, we present on-the-fly neural network NAMD (N^2AMD), a general machine learning framework that resolves the longstanding cost-accuracy dilemma in solid-state NAMD. Building upon an E(3)-equivariant neural network representation of the electronic Hamiltonian, our approach provides direct access to the exact excited-state forces and NACVs required for trajectory propagation through the learned Hamiltonian and its derivatives. This fundamentally obviates the CPA, making true on-the-fly NAMD in periodic solids a reality. We demonstrate that this framework achieves *ab initio* accuracy across diverse semiconductors at a fraction of the computational cost, opening the vast, uncharted landscape of strong electron-phonon coupling and nonequilibrium phase engineering to predictive theoretical exploration.

In NAMD simulations within the framework of density-functional theory (DFT) [12,28], the time-dependent electron wave function is expanded in the basis of instantaneous adiabatic Kohn-Sham (KS) orbitals $\Psi(\mathbf{r},\mathbf{R},t) = \sum_n C_n(t)\psi_n[\mathbf{r},\mathbf{R}(t)]$. The wave function evolves according to the time-dependent Schrödinger equation,

$$i\hbar\dot{C}_m(t) = \sum_n C_n(t)(\epsilon_m\delta_{mn} - i\hbar\mathbf{d}_{mn}\times\dot{\mathbf{R}}), \qquad (1)$$

where $\epsilon_n = \langle\psi_n|\hat{H}|\psi_n\rangle$ is the nth KS eigenenergy and $\mathbf{d}_{mn} = \langle\psi_m|\nabla_{\mathbf{R}}|\psi_n\rangle$ represents the nonadiabatic coupling vector (NACV) between states m and n. The coupled nuclear dynamics are governed by Newton's equations of motion: $\mathbf{F} = M\ddot{\mathbf{R}}$. Under the standard CPA, the backreaction of the excited charge carriers on the lattice is neglected, restricting the nuclear forces to those of the ground state $\mathbf{F} \approx \mathbf{F}_{gs}$ [Fig. 1(a)]. To overcome this limitation and accurately describe the coupled dynamics of both subsystems, we compute the excited-state PESs using the delta self-consistent field (Δ-SCF) approach [29]. This method has demonstrated significant success in both condensed matter physics and quantum chemistry as a robust tool for investigating electronic excited states [30–32]. Within the one-body band-excitation picture, for an excited state involving transitions from valence bands $\{i\}$ to conduction bands $\{a\}$ with occupation numbers $\{f_i\}$ and $\{f_a\}$, respectively, the force is given by

$$\mathbf{F} \approx \mathbf{F}_{\mathrm{gs}} + \sum_{i\in\mathrm{VB}}(1-f_i)\nabla_{\mathbf{R}}\varepsilon_i - \sum_{a\in\mathrm{CB}} f_a\nabla_{\mathbf{R}}\varepsilon_a \qquad (2)$$

Here, the total force is expressed as the sum of the ground-state force and the difference in KS orbital gradients. The double-counting energies vanish upon differentiation, as they do not explicitly depend on atomic positions. The formalism effectively decouples the ground-state and excitation energy scales, not only allowing for a direct assessment of the dynamical effects neglected by the CPA but also providing an efficient and robust framework for integration with neural networks. The primary approximation in this approach is the neglect of the self-consistent relaxation of the electronic Hamiltonian in response to the excited charge density. Nevertheless it remains valid for most nonstrongly correlated solids (as demonstrated in the "Benchmarks" section). By expanding the adiabatic KS orbitals in a numerical atomic orbital basis $\{\phi_\mu\}$ with coefficients $\{c_{i\mu}\}$, the orbital gradients in Eq. (2) are evaluated as [detailed derivation in Supplemental Material (SM) [33] Sec. 1]

$$-\nabla_{\mathbf{R}}\epsilon_i = \sum_{\mu\nu} c^*_{i\mu}c_{i\nu}\times[-\nabla_{\mathbf{R}}H_{\mu\nu} + \epsilon_i\nabla_{\mathbf{R}}S_{\mu\nu}], \qquad (3)$$

where $H_{\mu\nu} = \langle\phi_\mu|\hat{H}|\phi_\nu\rangle, S_{\mu\nu} = \langle\phi_\mu|\phi_\nu\rangle$ are Hamiltonian and overlap matrices. Note that explicit k-point indices are omitted in this formalism because, in the current implementation, our NAMD simulations employ large supercells, allowing electronic structure calculations to be safely restricted to a single k point (the Γ point). Beyond the neglect of excited-state forces, the CPA also fails to account for lattice heating resulting from carrier transitions, as it typically relies on a simple Boltzmann scaling of transition probabilities to mimic thermal equilibrium [47]. In contrast, on-the-fly NAMD explicitly conserves total energy during transitions by rescaling the nuclear velocities at each hopping event: $\dot{\mathbf{R}}' = \dot{\mathbf{R}} - (\sigma_{mn}/M)\mathbf{d}_{mn}$. Such adjustment is applied along the direction of the NACVs, which can be obtained by [34] (detailed derivation in SM [33] Sec. 1)

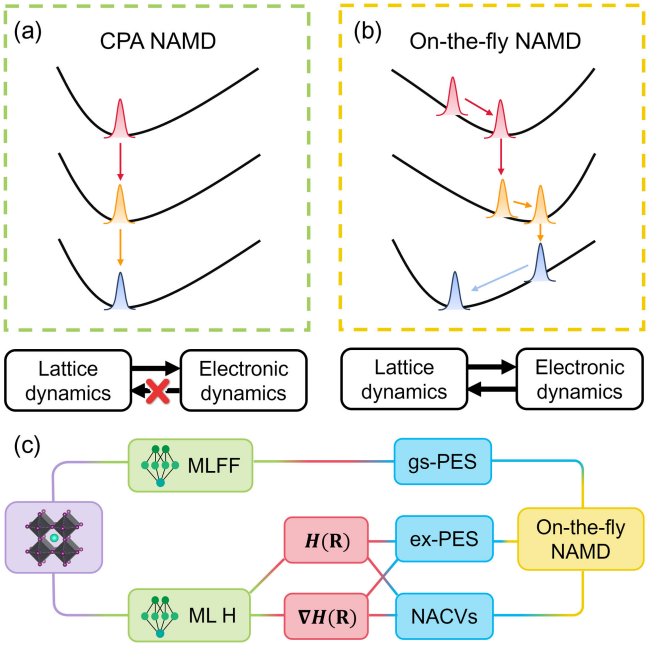

FIG. 1. (a) Conventional NAMD (CPA) in solids restricts nuclear motion to a static PES. (b) On-the-fly NAMD allows nuclei to evolve on excited-state (ex) PESs dictated by electronic transitions, closing the loop of coupled electron-nuclear interactions. (c) The on-the-fly N^{2}AMD work flow: an equivariant neural network predicts the electronic Hamiltonian, with nuclear derivatives obtained via automatic differentiation. Subsequently, ex-PESs and NACVs are derived from these outputs [Eqs. (2) and (4)] and combined with the machine learning force field-predicted ground-state potential energy surface to drive the full NAMD simulation.

$$\begin{aligned}\mathbf{d}_{mn} = \langle\psi_m|\nabla_{\mathbf{R}}|\psi_n\rangle &= -\frac{1}{\epsilon_m-\epsilon_n}\langle\psi_m|\nabla_{\mathbf{R}}\hat{H}|\psi_n\rangle \\ &= \frac{1}{\epsilon_m-\epsilon_n}\sum_{\mu\nu}c^*_{m\mu}c_{n\nu} \\ &\quad\times[-\nabla_{\mathbf{R}}H_{\mu\nu}+\epsilon_n\langle\nabla_{\mathbf{R}}\phi_\mu|\phi_\nu\rangle \\ &\quad+\epsilon_m\langle\phi_\mu|\nabla_{\mathbf{R}}\phi_\nu\rangle]\ m\neq n. \qquad (4)\end{aligned}$$

Implementing NAMD beyond the CPA requires the repetitive evaluation of Hamiltonian gradients for excited-state forces and NACVs, a task that becomes computationally prohibitive via density-functional perturbation theory. Our on-the-fly N^{2}AMD framework circumvents this bottleneck by leveraging E(3)-equivariant neural networks [Fig. 1(c)]. While we retain the foundational ML building blocks, including the HamGNN electronic Hamiltonian [35] and a dedicated ground-state ML interatomic potential Allegro [36], from our previous work [22], the present work orchestrates them into a fundamentally different on-the-fly methodology. (See detailed comparison between two work flows in SM [33], Sec. 11) As the first step of this work flow, we employ HamGNN to construct deep neural Hamiltonians directly from instantaneous atomic configurations, bypassing iterative DFT cycles while rigorously preserving geometric symmetries. Upon diagonalizing the predicted Hamiltonian matrices to recover the KS energies ϵ_i and orbitals ψ_i, the work flow proceeds to evaluate the matrix gradients required for force and coupling calculations [Eqs. (2) and (4)]. These are efficiently obtained by computing the Hamiltonian gradient $\nabla_{\mathbf{R}}H_{\mu\nu}$ via forward-mode automatic differentiation, alongside the overlap matrix gradient $\langle\nabla_{\mathbf{R}}\phi_\mu|\phi_\nu\rangle$ and $\langle\phi_\mu|\nabla_{\mathbf{R}}\phi_\nu\rangle$ using a two-center integral technique. Finally, efficient NAMD can be executed by combining these key quantities with the ground-state PES predicted by Allegro. Crucially, this hybrid "delta-prediction" architecture decouples the extensive ground-state PES from the intensive excitation contributions derived from the neural Hamiltonian. This separation resolves the fundamental scaling conflict inherent to extended systems, ensuring physical consistency and transferability while maximizing computational efficiency (see SM [33] Sec. 2 for work flow details).

Benchmarks—We first validate the excited-state force formalism [Eq. (2)] using bulk silicon, a prototypical semiconductor. To simulate a nonequilibrium regime with nonzero forces, atoms in a 64-atom supercell are randomly displaced from ideal lattice positions with 0.02 Å. As shown in Fig. 2(a), promoting one single electron from the valence band maximum (VBM) to the conduction band minimum (CBM) induces a significant reshaping of the PES. Our formalism captures this shift with exceptional fidelity, agreeing with rigorous, self-consistent Δ-SCF benchmarks to within a mean absolute error (MAE) of 7.6 meV/Å. In contrast, the ground-state approximation (CPA) yields a discrepancy of 110.4 meV/Å, confirming that the CPA introduces substantial errors under relatively strong photoexcitation (here, 0.39% of the valence electrons excited). Computational efficiency is benchmarked in Fig. 2(b). For a 96-atom silicon system, on-the-fly N^{2}AMD reduces the wall time per ionic step on one Intel(R) Xeon (R) Max 9462 @ 2.7 GHz CPU from 4.14 h by DFT to 91.43 s, achieving a speedup of 163×. This advantage grows with system size, as our framework exhibits $\mathcal{O}(N^2)$ scaling, whereas DFT follows a much steeper trajectory. It is worth noting that the observed scaling is determined by our current implementation, which employs the full Hamiltonian matrix and its derivatives. Future algorithmic refinements leveraging the physical principle of "nearsightedness," specifically by exploiting matrix sparsity and symmetry, could significantly reduce this scaling for large-scale simulations (see SM [33] Sec. 3 for a detailed comparison of the scaling behaviors).

We next assess the accuracy of the on-the-fly N^{2}AMD framework in predicting essential NAMD components. The deep neural Hamiltonian reproduces DFT-computed real-space matrices with an MAE of 0.045 meV and yields a closely matched band structure [SM [33], Figs. S2(a) and

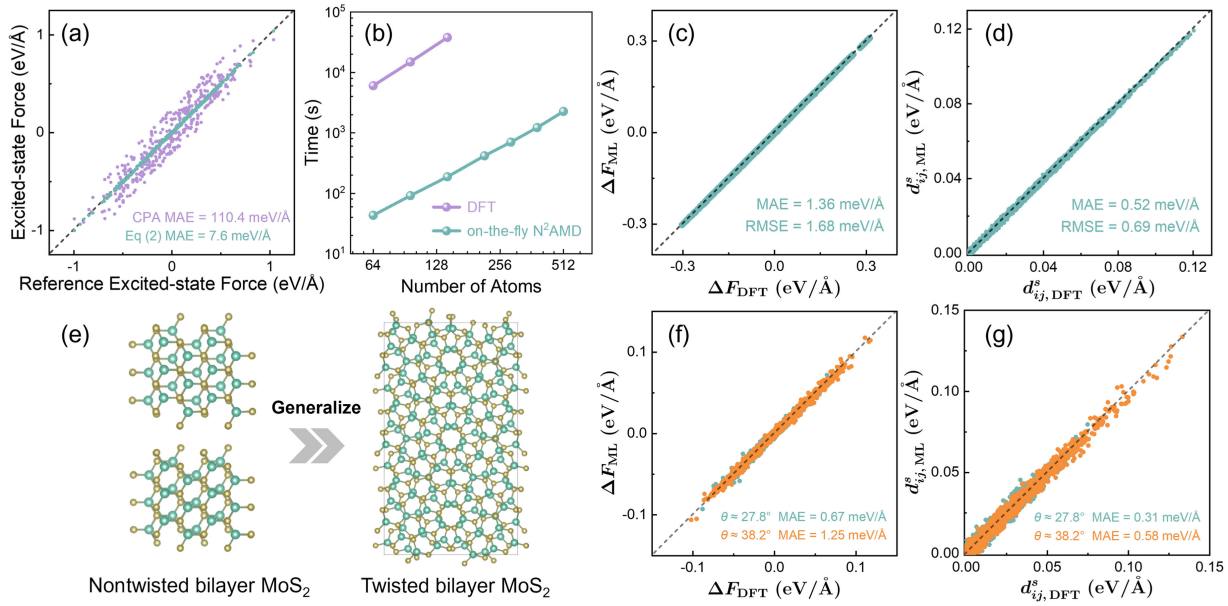

FIG. 2. Accuracy, efficiency, and transferability of on-the-fly N^{2}AMD. (a)–(d) Benchmarks on bulk silicon. (a) A comparison of reference Δ-SCF excited-state forces against N^{2}AMD predictions [Eq. (2), cyan] and the ground-state approximation (purple). (b) Computational time per ionic step for different sized systems. (c) Prediction accuracy for the excitation force contribution $\Delta\mathbf{F} = \mathbf{F}_{\mathrm{ex}} - \mathbf{F}_{\mathrm{gs}}$, and (d) for the magnitudes of smoothed NACVs d^s_{ij}. (e)–(g) Transferability demonstration on bilayer MoS_2. N^{2}AMD is trained exclusively on nontwisted configurations and evaluated on unseen twisted structures with varying angles θ.

S2(b)]. Building on this foundation, we evaluate the critical ingredients for NAMD beyond the CPA: excited-state forces and NACVs. For seven states around the Fermi surface, on-the-fly N^{2}AMD accurately captures the differences between ground- and excited-state forces $\Delta\mathbf{F} = \mathbf{F}_{\mathrm{ex}} - \mathbf{F}_{\mathrm{gs}}$, yielding an MAE of 1.36 meV/Å [Fig. 2(c)]. As for NACVs, we target the magnitude of smoothed NACVs defined as $\mathbf{d}^s_{ij} = |(\epsilon_i - \epsilon_j)\mathbf{d}_{ij}|$ to migrate to issues associated with its numerical instabilities near accidental energy degeneracies and the arbitrary phases of KS wave functions. It is found that our framework is capable of predicting couplings between selected state pairs with extremely high fidelity [Fig. 2(d); MAE, 0.52 meV/Å].

We further compare our on-the-fly N^{2}AMD framework against standard CPA NAMD by investigating hole relaxation dynamics in a type-II MoS_2/WS_2 heterostructure [SM [33], Fig. S4(b)]. Although both methods identify the same relaxation pathway (MoS_2@K → WS_2@K → WS_2@Γ), significant discrepancies emerge in the kinetics [SM [33], Figs. S4(c)–S4(f)]. CPA NAMD suggests carrier trapping at the intermediate WS_2@K state [SM [33], Fig. S4(c)], resulting in a dramatic underestimation of the relaxation rate. In contrast, on-the-fly N^{2}AMD correctly captures the rapid decay to the final WS_2@Γ. This improvement arises from the complete treatment of electron-phonon coupling, which captures the generation of nonequilibrium phonon populations that drive efficient energy dissipation. To ensure a rigorous comparison, both methods employ nonadiabatic coupling phase corrections [37], preventing the artificial acceleration noted in earlier work [38]. The superior performance of N^{2}AMD is thus strictly attributable to the inclusion of explicit excited-state forces.

Finally, we demonstrate the framework's transferability across diverse solid-state systems. Two challenging scenarios were tested: (i) moiré physics in bilayer MoS_2 [Figs. 2(e)–2(g)], where a model trained exclusively on nontwisted bilayers successfully generalizes to twisted structures; and (ii) configurational disorder and variable stoichiometry (the Ga/Al mixing ratio x) in the solid solution $Ga_xAl_{1-x}As$ [SM [33], Figs. S3(e)–S3(g)], where a model trained on configurations with $x = 0, 1/4, 2/4, 3/4$, and 1 accurately predicts unseen compositions ($x = 3/8, 5/8$). In both cases, excited-state forces and NACVs are reproduced with meV/Å- or sub-meV/Å-level accuracy, ensuring robust simulation of far-from-equilibrium dynamics in novel materials.

Application 1: Photoinduced ferroelectric switching—We next apply on-the-fly N^{2}AMD to a regime fundamentally inaccessible to the conventional CPA NAMD in solids: photoinduced phase transitions driven by the reshaping of excited-state potential energy landscapes. A prime example of this regime is sliding ferroelectricity, a promising route for next-generation nonvolatile memory [48] where ultrafast manipulation via laser pulses requires accurate theoretical simulation [49–53]. We investigate photoinduced ferroelectric switching in bilayer hexagonal boron nitride (*h*-BN), focusing on how photoexcitation tunes the energy barrier between AB and BA stacking orders. In our periodic models, the photoexcitation is appropriately quantified by the excitation density. Static

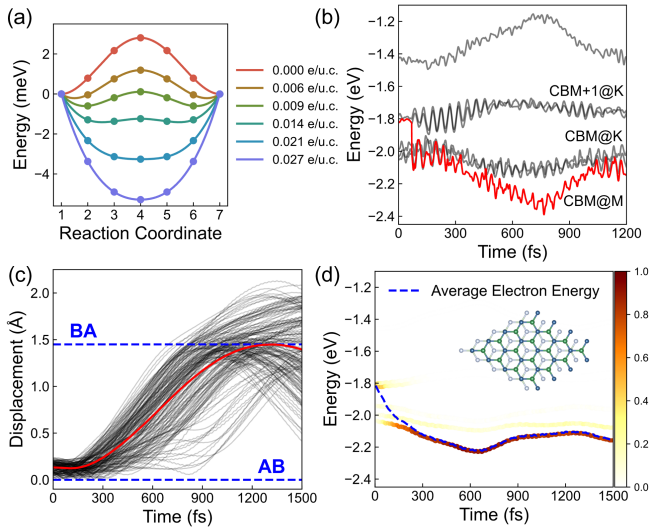

FIG. 3. Photoinduced ferroelectric switching in bilayer *h*-BN. (a) Potential energy curves along the AB-BA transition pathway under varying photoexcitation densities (0.000–0.027 excited electrons per unit cell). Energies of the equilibrium AB and BA states are set at zero. (b)–(d) On-the-fly N^2AMD results. (b) KS eigenvalue evolution in one representative trajectory with electron hopping (red curve). (c) In-plane sliding displacement progressions across the trajectory ensemble relative to equilibrium AB and BA states (blue dashed lines), ensemble average displacement (red line). (d) Average electron energy evolution, with the color scale indicating the per-state excited electron population.

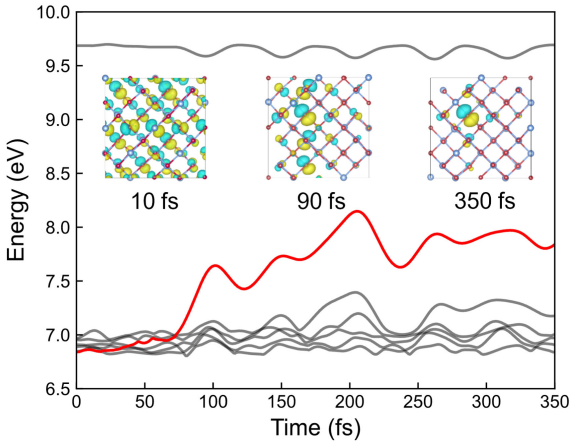

FIG. 4. Real-time evolution of carrier localization in anatase TiO_2 demonstrating ultrafast polaron formation. Lines from bottom to top: states from VBM-5 to VBM, and the CBM. Insets: hole-hosting state wave functions at 10, 90, and 350 fs.

calculations show that an excitation density of 0.027 e/u.c. eliminates the barrier entirely, creating a driving force for spontaneous switching [Fig. 3(a)]. Simulations at this excitation concentration, 100 K, reveal a stark dichotomy between methods. CPA NAMD predicts zero switching events within 1.5 ps [SM [33], Fig. S5(b)]. Conversely, on-the-fly N^2AMD suggests that 82% of trajectories undergo a complete polarization reversal (in-plane displacement reaches $\xi = 1.45$ Å) in the same time frame [Fig. 3(c)]. Analysis of a representative trajectory reveals that the CBM@M KS eigenvalue drops significantly between 300 and 800 fs before recovering, providing the requisite force for lattice sliding [Fig. 3(b)]. In contrast, CPA NAMD eigenvalues merely oscillate around equilibrium [SM [33], Fig. S5(a)]. Notably, both methods capture an initial rapid (200 fs) electron relaxation from CBM + 1@K to CBM@M [Fig. 3(d) and SM [33], Fig. S5(c)], which explains the brief displacement plateau preceding sliding. To further validate the necessity of our approach, one constrained Born-Oppenheimer molecular dynamics simulation is also performed [SM [33], Figs. S5(d)–S5(f)]. While it correctly predicts the sliding, it inherently fails to describe the critical hot-carrier cooling observed in NAMD results. Thus, on-the-fly N^2AMD resolves the complete mechanism surpassing both CPA NAMD and constrained Born-Oppenheimer molecular dynamics.

Application 2: Quasiparticle formation dynamics—Finally, we demonstrate the capacity of on-the-fly N^2AMD to capture quasiparticle dynamics at the hybrid functional level. Although the extreme computational cost of hybrid functionals generally limits conventional NAMD and Ehrenfest dynamics of extended solids to the Perdew-Burke-Ernzerhof functional [39], our framework leverages deep neural Hamiltonians to incorporate hybrid functional accuracy without the associated computational bottleneck. We apply this approach to investigate the formation of small hole polarons in anatase TiO_2, a process where mitigating self-interaction errors via hybrid functionals is critical, yet historically intractable for NAMD [40,54]. Static Heyd-Scuseria-Ernzerhof functional [41] calculations identify a polaron state 0.77 eV above the VBM, characterized by a *p*-orbital shaped wave function centered on an oxygen atom with 0.14 Å lattice distortions [SM [33], Figs. S6(a) and S6(b)]. Our simulation provides a time-resolved view of its formation. Following photoexcitation, the hot hole relaxes to the VBM within 70 fs, then rapidly plunges into the band gap, entering the self-trapping state (Fig. 4, red line). The hole wave function transitions from delocalized at 10 fs to highly localized at 90 fs, achieving a stable polaron configuration by 350 fs (insets, Fig. 4). By rendering such demanding simulations feasible, on-the-fly N^2AMD offers a powerful tool to explore complicated polaron-mediated dynamics.

In conclusion, on-the-fly N^2AMD resolves the long-standing computational bottleneck prohibiting exact nonadiabatic molecular dynamics in extended systems. By mapping the *ab initio* electronic Hamiltonian to an E(3)-equivariant neural network, we restore the essential feedback loop between excited carriers and the lattice without the prohibitive scaling of density functional theory. The method's versatility is evidenced by its successful application to distinct nonequilibrium regimes, including

correcting hot carrier relaxation rates in heterostructures, driving nonthermal phase transitions in ferroelectrics, and capturing self-trapping polaron dynamics in oxides. This framework bridges the gap between static electronic structure and nonequilibrium dynamics, paving the way for the first-principles design and discovery of materials operating far from equilibrium.

Acknowledgments—We thank Dr. Daye Zheng for implementing overlap gradient outputs in ABACUS. We acknowledge support from the National Natural Science Foundation of China (No. 12188101, No. 12274081, No. 11991061, No. 22333003, No. 22361132528, No. 12271109, and No. 12526211), Shanghai Science and Technology Program (No. 23JC1400900), National Key Research and Development Program of China (No. 2024YFA1409800), Shanghai Pilot Program for Basic Research—Fudan University 21TQ1400100 (No. 22TQ017), Scientific Research Innovation Capability Support Project for Young Faculty (No. SRICSPYF-ZY2025159), and Xuemin Institute of Advanced Studies, Fudan University. O. V. P acknowledges the support from the U.S. National Science Foundation (No. CHE-2603101). X. G. G. acknowledges support of the Innovation Program for Quantum Science and Technology (No. 2024ZD0300100).

Data availability—The source code of on-the-fly N^2AMD, the raw data, and an example case with detailed instructions on how to use our code are available at Zenodo [55].

[1] F. Williams and A. J. Nozik, Solid-state perspectives of the photoelectrochemistry of semiconductor–electrolyte junctions, Nature (London) **312**, 21 (1984).
[2] M. Volkov, S. A. Sato, F. Schlaepfer, L. Kasmi, N. Hartmann, M. Lucchini, L. Gallmann, A. Rubio, and U. Keller, Attosecond screening dynamics mediated by electron localization in transition metals, Nat. Phys. **15**, 1145 (2019).
[3] A. V. Akimov, A. J. Neukirch, and O. V. Prezhdo, Theoretical insights into photoinduced charge transfer and catalysis at oxide interfaces, Chem. Rev. **113**, 4496 (2013).
[4] V. A. Jhalani, J.-J. Zhou, and M. Bernardi, Ultrafast hot carrier dynamics in GaN and its impact on the efficiency droop, Nano Lett. **17**, 5012 (2017).
[5] R. Long, O. V. Prezhdo, and W. Fang, Nonadiabatic charge dynamics in novel solar cell materials, WIREs Comput. Mol. Sci. **7**, e1305 (2017).
[6] M. Guan, D. Chen, S. Hu, H. Zhao, P. You, and S. Meng, Theoretical insights into ultrafast dynamics in quantum materials, Ultrafast Science, 10.34133/2022/9767251 (2022).
[7] L. Wang, J. Qiu, X. Bai, and J. Xu, Surface hopping methods for nonadiabatic dynamics in extended systems, WIREs Comput. Mol. Sci. **10**, e1435 (2020).
[8] J. C. Tully, Molecular dynamics with electronic transitions, J. Chem. Phys. **93**, 1061 (1990).
[9] T. R. Nelson, A. J. White, J. A. Bjorgaard, A. E. Sifain, Y. Zhang, B. Nebgen, S. Fernandez-Alberti, D. Mozyrsky, A. E. Roitberg, and S. Tretiak, Non-adiabatic excited-state molecular dynamics: Theory and applications for modeling photophysics in extended molecular materials, Chem. Rev. **120**, 2215 (2020).
[10] I. Polyak, L. Hutton, R. Crespo-Otero, M. Barbatti, and P. J. Knowles, Ultrafast photoinduced dynamics of 1,3-cyclohexadiene using XMS-CASPT2 surface hopping, J. Chem. Theory Comput. **15**, 3929 (2019).
[11] S. Mai, P. Marquetand, and L. González, Nonadiabatic dynamics: The SHARC approach, WIREs Comput. Mol. Sci. **8**, e1370 (2018).
[12] A. V. Akimov and O. V. Prezhdo, The PYXAID program for non-adiabatic molecular dynamics in condensed matter systems, J. Chem. Theory Comput. **9**, 4959 (2013).
[13] B. Smith and A. V. Akimov, Modeling nonadiabatic dynamics in condensed matter materials: Some recent advances and applications, J. Phys. Condens. Matter **32**, 073001 (2019).
[14] X.-Y. Liu, D. Xiao, W.-H. Fang, and G. Cui, Excited-state wave functions and energies predicted by machine learning based on graph neural networks, J. Chem. Theory Comput. **21**, 9009 (2025).
[15] M. Shakiba and A. V. Akimov, Machine-learned Kohn–Sham Hamiltonian mapping for nonadiabatic molecular dynamics, J. Chem. Theory Comput. **20**, 2992 (2024).
[16] J. Westermayr, M. Gastegger, and P. Marquetand, Combining SchNet and SHARC: The SchNarc machine learning approach for excited-state dynamics, J. Phys. Chem. Lett. **11**, 3828 (2020).
[17] P. O. Dral, F. Ge, Y.-F. Hou, P. Zheng, Y. Chen, M. Barbatti, O. Isayev, C. Wang, B.-X. Xue, M. Pinheiro Jr, Y. Su, Y. Dai, Y. Chen, L. Zhang, S. Zhang, A. Ullah, Q. Zhang, and Y. Ou, MLatom 3: A platform for machine learning-enhanced computational chemistry simulations and workflows, J. Chem. Theory Comput. **20**, 1193 (2024).
[18] S. Mausenberger, C. Müller, A. Tkatchenko, P. Marquetand, L. González, and J. Westermayr, SPAINN: Equivariant message passing for excited-state nonadiabatic molecular dynamics, Chem. Sci. **15**, 15880 (2024).
[19] J. Li, P. Reiser, B. R. Boswell, A. Eberhard, N. Z. Burns, P. Friederich, and S. A. Lopez, Automatic discovery of photoisomerization mechanisms with nanosecond machine learning photodynamics simulations, Chem. Sci. **12**, 5302 (2021).
[20] Z. Wang, J. Dong, J. Qiu, and L. Wang, All-atom nonadiabatic dynamics simulation of hybrid graphene nanoribbons based on Wannier analysis and machine learning, ACS Appl. Mater. Interfaces **14**, 22929 (2022).
[21] D. Liu, B. Wang, Y. Wu, A. S. Vasenko, and O. V. Prezhdo, Breaking the size limitation of nonadiabatic molecular dynamics in condensed matter systems with local descriptor machine learning, Proc. Natl. Acad. Sci. U.S.A. **121**, e2403497121 (2024).
[22] C. Zhang, Y. Zhong, Z.-G. Tao, X. Qin, H. Shang, Z. Lan, O. V. Prezhdo, X.-G. Gong, W. Chu, and H. Xiang, Advancing nonadiabatic molecular dynamics simulations in solids with E(3) equivariant deep neural Hamiltonians, Nat. Commun. **16**, 2033 (2025).

[23] M. Martyka, X.-Y. Tong, J. Jankowska, and P. O. Dral, OMNI-P2x: A universal neural network potential for excited-state simulations, 10.26434/chemrxiv-2025-j207x (2025).
[24] R. Barrett, C. Ortner, and J. Westermayr, Transferable Machine Learning Potential X-MACE for Excited States using Integrated DeepSets, arXiv:2502.12870.
[25] J. Martinka, L. Zhang, Y.-F. Hou, M. Martyka, J. Pittner, M. Barbatti, and P. O. Dral, A Descriptor Is All You Need: Accurate Machine Learning of Nonadiabatic Coupling Vectors, arXiv:2505.23344.
[26] X. Li, N. Lubbers, S. Tretiak, K. Barros, and Y. Zhang, Machine learning framework for modeling exciton polaritons in molecular materials, J. Chem. Theory Comput. **20**, 891 (2024).
[27] S. Axelrod, E. Shakhnovich, and R. Gómez-Bombarelli, Excited state non-adiabatic dynamics of large photoswitchable molecules using a chemically transferable machine learning potential, Nat. Commun. **13**, 3440 (2022).
[28] C. F. Craig, W. R. Duncan, and O. V. Prezhdo, Trajectory surface hopping in the time-dependent Kohn-Sham approach for electron-nuclear dynamics, Phys. Rev. Lett. **95**, 163001 (2005).
[29] J. Gavnholt, Delta self-consistent field method to obtain potential energy surfaces of excited molecules on surfaces, Phys. Rev. B **78**, 075441 (2008).
[30] W. Yang and P. W. Ayers, Foundation for the δSCF Approach in Density Functional Theory, arXiv:2403.04604.
[31] C. Gao, L. Zhang, Q. Zheng, and J. Zhao, Tuning the lifetime of photoexcited small polarons on rutile TiO_2 surface via molecular adsorption, J. Phys. Chem. C **125**, 27275 (2021).
[32] E. Vandaele, M. Mališ, and S. Luber, The δSCF method for non-adiabatic dynamics of systems in the liquid phase, J. Chem. Phys. **156**, 130901 (2022).
[33] See Supplemental Material at http://link.aps.org/supplemental/10.1103/9wbw-h87d for computational and training details, additional benchmarks, a detailed derivation and algorithmic flowchart of on-the-fly N^2AMD, a comprehensive comparison with our previous work and further discussions, which includes Refs. [22,34–46].
[34] E. Abad, J. P. Lewis, V. Zobač, P. Hapala, P. Jelínek, and J. Ortega, Calculation of non-adiabatic coupling vectors in a local-orbital basis set, J. Chem. Phys. **138**, 154106 (2013).
[35] Y. Zhong, H. Yu, M. Su, X. Gong, and H. Xiang, Transferable equivariant graph neural networks for the Hamiltonians of molecules and solids, npj Comput. Mater. **9**, 1 (2023).
[36] A. Musaelian, S. Batzner, A. Johansson, L. Sun, C. J. Owen, M. Kornbluth, and B. Kozinsky, Learning local equivariant representations for large-scale atomistic dynamics, Nat. Commun. **14**, 579 (2023).
[37] A. V. Akimov, A simple phase correction makes a big difference in nonadiabatic molecular dynamics, J. Phys. Chem. Lett. **9**, 6096 (2018).
[38] Q. Zheng, W. A. Saidi, Y. Xie, Z. Lan, O. V. Prezhdo, H. Petek, and J. Zhao, Phonon-assisted ultrafast charge transfer at van der Waals heterostructure interface, Nano Lett. **17**, 6435 (2017).
[39] J. P. Perdew, K. Burke, and M. Ernzerhof, Generalized gradient approximation made simple, Phys. Rev. Lett. **77**, 3865 (1996).
[40] A. R. Elmaslmane, M. B. Watkins, and K. P. McKenna, First-principles modeling of polaron formation in TiO_2 polymorphs, J. Chem. Theory Comput. **14**, 3740 (2018).
[41] J. Heyd, G. E. Scuseria, and M. Ernzerhof, Hybrid functionals based on a screened Coulomb potential, J. Chem. Phys. **118**, 8207 (2003).
[42] P. Pulay, *Ab initio* calculation of force constants and equilibrium geometries in polyatomic molecules: I. Theory, Mol. Phys. **17**, 197 (1969).
[43] F. Chen, T. Ma, T. Zhang, Y. Zhang, and H. Huang, Atomic-level charge separation strategies in semiconductor-based photocatalysts, Adv. Mater. **33**, 2005256 (2021).
[44] T. Ozaki, Variationally optimized atomic orbitals for large-scale electronic structures, Phys. Rev. B **67**, 155108 (2003).
[45] P. Lin, X. Ren, X. Liu, and L. He, *Ab initio* electronic structure calculations based on numerical atomic orbitals: Basic fomalisms and recent progresses, WIREs Comput. Mol. Sci. **14**, e1687 (2024).
[46] P. Lin, X. Ren, and L. He, Accuracy of localized resolution of the identity in periodic hybrid functional calculations with numerical atomic orbitals, J. Phys. Chem. Lett. **11**, 3082 (2020).
[47] Q. Zheng, W. Chu, C. Zhao, L. Zhang, H. Guo, Y. Wang, X. Jiang, and J. Zhao, *Ab initio* nonadiabatic molecular dynamics investigations on the excited carriers in condensed matter systems, WIREs Comput. Mol. Sci. **9**, e1411 (2019).
[48] R. Bian, R. He, E. Pan, Z. Li, G. Cao, P. Meng, J. Chen, Q. Liu, Z. Zhong, W. Li, and F. Liu, Developing fatigue-resistant ferroelectrics using interlayer sliding switching, Science **385**, 57 (2024).
[49] E. J. Sie, C. M. Nyby, C. D. Pemmaraju, S. J. Park, X. Shen, J. Yang, M. C. Hoffmann, B. K. Ofori-Okai, R. Li, A. H. Reid, S. Weathersby, E. Mannebach, N. Finney, D. Rhodes, D. Chenet, A. Antony, L. Balicas, J. Hone, T. P. Devereaux, T. F. Heinz, X. Wang, and A. M. Lindenberg, An ultrafast symmetry switch in a Weyl semimetal, Nature (London) **565**, 61 (2019).
[50] L. Gao and L. Bellaiche, Large photoinduced tuning of ferroelectricity in sliding ferroelectrics, Phys. Rev. Lett. **133**, 196801 (2024).
[51] Q. Yang and S. Meng, Light-induced complete reversal of ferroelectric polarization in sliding ferroelectrics, Phys. Rev. Lett. **133**, 136902 (2024).
[52] Z.-G. Tao, S. Deng, O. V. Prezhdo, H. Xiang, W. Chu, and X.-G. Gong, Tunable ultrafast charge transfer across homojunction interface, J. Am. Chem. Soc. **146**, 24016 (2024).
[53] D. Yao, Z.-G. Tao, C. Zhang, L. Peng, X.-G. Gong, and W. Chu, Reprogrammable carrier lifetimes in 2D materials via ultrafast ferroelectric switching, J. Am. Chem. Soc. **147**, 46197 (2025).
[54] C. Franchini, M. Reticcioli, M. Setvin, and U. Diebold, Polarons in materials, Nat. Rev. Mater. **6**, 560 (2021).
[55] C. Zhang, Y. Zhong, Z.-G. Tao, Y. Li, Z. Lan, O. V. Prezhdo, X.-G. Gong, W. Chu, and H. Xiang, QDyn code and original data for "Nonadiabatic Molecular Dynamics on Real-time Excited-State Surfaces via Machine Learning Hamiltonians", Zenodo, 10.5281/zenodo.20272172 (2026).